# Bismuth Telluride (Bi 2 Te 3 ) Nanowires: Synthesis by Cyclic Electrodeposition/Stripping, Thinning by Electrooxidation, and Electrical Power Generation †

**ARTICLE** *in* LANGMUIR · JANUARY 2007

Impact Factor: 4.46 · DOI: 10.1021/la061275g · Source: PubMed

# Bismuth Telluride ($Bi_2Te_3$) Nanowires: Synthesis by Cyclic Electrodeposition/Stripping, Thinning by Electrooxidation, and Electrical Power Generation†

E. J. Menke, M. A. Brown, Q. Li, J. C. Hemminger, and R. M. Penner*

*Institute for Surface and Interface Science and Department of Chemistry, University of California, Irvine, California 92679-2025*

*Received May 7, 2006. In Final Form: June 30, 2006*

Nanowires composed of the thermoelectric material $Bi_2Te_3$ were synthesized on highly oriented pyrolytic graphite (HOPG) electrodes using the electrochemical step edge decoration (ESED) method. Nanowire synthesis was initiated by applying a voltage pulse of −0.75 V versus SCE for 5 ms to an HOPG electrode in an aqueous solution containing both $Bi^{3+}$ and $TeO_2^{2-}$, thereby producing nuclei at the step edges. $Bi_2Te_3$ was electrodeposited onto these nuclei using a cyclic electrodeposition−stripping scheme that involved the electrodeposition of bismuth-rich $Bi_2Te_3$ on a negative-going voltammetric scan (to −0.05 V) and the subsequent anodic stripping of excess bismuth from these nanowires during a positive-going scan (to +0.35 V). When this cycle was repeated 10−50 times, $Bi_2Te_3$ nanowires in the 100−300-nm-diameter range were obtained. These nanowires were narrowly dispersed in diameter ($RSD_{dia}$ = 10−20%), were more than 100 $\mu$m in length, and were organized into parallel arrays containing hundreds of wires. Smaller nanowires, with diameters down to 30 nm, were obtained by electrooxidizing 150-nm-diameter $Bi_2Te_3$ nanowires at +0.37 V under conditions of kinetic control. This oxidation process unexpectedly improved the uniformity of $Bi_2Te_3$ nanowires, and X-ray photoelectron spectroscopy (XPS) shows that these nanowires retain a $Bi_2Te_3$ core but also have a thin surface layer composed of Bi and Te oxides. The ability of $Bi_2Te_3$ nanowires to generate electrical power was assessed by transferring ensembles of these nanowires onto cyanoacrylate-coated glass surfaces and evaporating 4-point nickel contacts. A dimensionless figure of merit, *ZT*, ranging from 0 to 0.85 was measured for fresh samples that were less than 1 day old. XPS reveals that $Bi_2Te_3$ nanowires are oxidized within a week to $Bi_2O_3$ and $TeO_2$. These oxides may interfere with the application by evaporation of electrical contacts to these nanowires.

## I. Introduction

In use for more than 50 years,[1] bismuth telluride ($Bi_2Te_3$) is still the benchmark against which the performance of other thermoelectric materials is compared, although its performance has been surpassed by other materials.[2,3] The efficiency of a particular thermoelectric material for power generation can be expressed in terms of the dimensionless quantity $ZT$[3]

$$ZT = \frac{S^2\sigma T}{\kappa} \quad (1)$$

where $Z$ is the thermoelectric figure of merit, $T$ is the mean temperature of the material, $S$ is the Seebeck coefficient, $\sigma$ is the electrical conductivity, and $\kappa$ is the thermal conductivity. $Bi_2Te_3$ and alloys with $Sb_2Te_3$ (p-doped) and $Bi_2Se_3$ (n-doped) have a room-temperature $ZT$ near 1.0. Higher $ZT$ values in the 2.0−2.5 range have been reported for multiple quantum well (MQW) structures based on $PbTe/PbSe_xTe_{1-x}$ and $Bi_2Te_3/Sb_2Te_3$ designed to impede lattice-based thermal transport.[4] These experimental successes come in the wake of theoretical studies suggesting that low-dimensional materials including quantum wells and nanowires may exhibit $ZT$ values that are considerably larger than 1.0 as a consequence of enhanced $S$ and $\sigma$[5−9] and/or depressed $\kappa$[10−15] relative to the corresponding properties of the bulk material.

One-dimensional systems should be even more effective at impeding thermal transport than two-dimensional MQW systems and even larger values for $ZT$ should therefore be accessible for nanowires, but few experimental measurements of $ZT$ for nanowires have been reported.[16] In the specific case of $Bi_2Te_3$ nanowires, we are aware of just one: by Shi and co-workers,[17,18] which yielded a value of $ZT$ = 0.02 (300 K) for nanowires with a diameter of 60 nm, composed of bismuth-rich $Bi_{0.485}Te_{0.515}$. This relatively low value was rationalized on the basis of the low Seebeck coefficient seen for this particular stoichiometry.[17,18] A second recent study[19] reports a measurement of $\kappa$ for 40-nm-diameter $Bi_2Te_3$ nanowires, and the result was estimated to be more than an order of magnitude lower than the thermal conductivity of bulk $Bi_2Te_3$. Especially in view of the number of syntheses of $Bi_2Te_3$ nanowires that have been carried out (see below), the paucity of these crucial thermal measurements suggests that these data are not easily obtained using the available materials.

How have these $Bi_2Te_3$ nanowires been synthesized? In most cases, the template synthesis method has been employed.[20−22] Martin,[23] Stacy,[19,24−29] and Wang[30,31] have electrodeposited $Bi_2$-

† Part of the Electrochemistry special issue.

* Corresponding author. E-mail: rmpenner@uci.edu.

(1) Goldsmit, H. J.; Douglas, R. W. *Br. J. Appl. Phys.* **1954**, *5*, 386.
(2) Chen, G.; Dresselhaus, M. S.; Dresselhaus, G.; Fleurial, J. P.; Caillat, T. *Int. Mater. Rev.* **2003**, *48*, 45.
(3) Tritt, T. M.; Subramanian, M. A. *MRS Bull.* **2006**, *31*, 188.
(4) Bottner, H.; Chen, G.; Venkatasubramanian, R. *MRS Bull.* **2006**, *31*, 211.
(5) Broido, D. A.; Reinecke, T. L. *Appl. Phys. Lett.* **1995**, *67*, 100.
(6) Broido, D. A.; Reinecke, T. L. *Phys. Rev. B* **1995**, *51*, 13797.
(7) Hicks, L. D.; Dresselhaus, M. S. *Phys. Rev. B* **1993**, *47*, 12727.
(8) Hicks, L. D.; Dresselhaus, M. S. *Phys. Rev. B* **1993**, *47*, 16631.
(9) Hicks, L. D.; Harman, T. C.; Dresselhaus, M. S. *Appl. Phys. Lett.* **1993**, *63*, 3230.
(10) Balandin, A. *Phys. Low-Dimens. Semicond. Struct.* **2000**, *1−2*, 1.
(11) Balandin, A.; Wang, K. L. *Phys. Rev. B* **1998**, *58*, 1544.
(12) Balandin, A.; Wang, K. L. *J. Appl. Phys.* **1998**, *84*, 6149.
(13) Walkauskas, S. G.; Broido, D. A.; Kempa, K.; Reinecke, T. L. *J. Appl. Phys.* **1999**, *85*, 2579.
(14) Zou, J.; Balandin, A. *J. Appl. Phys.* **2001**, *89*, 2932.
(15) Sur, I.; Casian, A.; Balandin, A. *Phys. Rev. B* **2004**, *69*.
(16) Rao, A. M.; Ji, X. H.; Tritt, T. M. *MRS Bull.* **2006**, *31*, 218.
(17) Shi, L.; Yu, C. H.; Zhou, J. H. *J. Phys. Chem. B* **2005**, *109*, 22102.
(18) Zhou, J. H.; Jin, C. G.; Seol, J. H.; Li, X. G.; Shi, L. *Appl. Phys. Lett.* **2005**, *87*.
(19) Borca-Tasciuc, D. A.; Chen, G.; Prieto, A.; Martin-Gonzalez, M. S.; Stacy, A.; Sands, T.; Ryan, M. A.; Fleurial, J. P. *Appl. Phys. Lett.* **2004**, *85*, 6001.

10.1021/la061275g CCC: $33.50 
Published on Web 08/16/2006

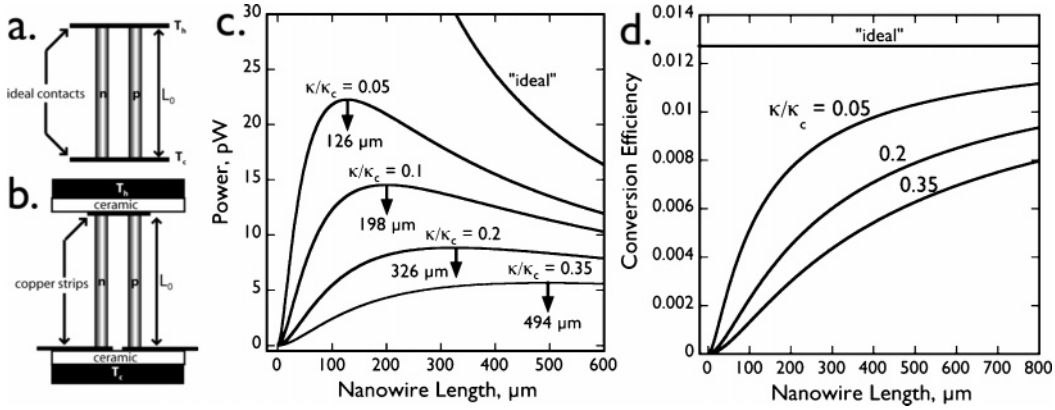


**Figure 1.** (a) Schematic diagram of a two-element thermoelectric device with ideal contacts that are maintained at $T_h$ and $T_c$. (b) Schematic diagram of a device with nonideal contacts that include an electrically insulating ceramic layer with a defined thickness, $L_c$, and thermal conductivity, $\kappa_c$. (c) Plot of total power generated, $P$, from the devices shown in a and b as a function of the nanowire length, $L_o$, for 100-nm-diameter nanowires. Shown are plots for four values of the ratio $\kappa/\kappa_c$, where $\kappa$ and $\kappa_c$ are the thermal conductivities of the nanowires and the thermal contacts, respectively. The power produced by a device with ideal contacts is given by $P_{ideal} = (\alpha^2/\rho)(\Delta T^2/2)(A/L_o)$, where for $Bi_2Te_3$ at 300 K, $\alpha$ (the Seebeck coefficient) $= 2.00 \times 10^{-4}$ V/K, $\rho$ (the nanowire electrical resistivity) $= 0.001\ \Omega$ cm, $\Delta T = 25$ K, and $A$ is the cross-sectional area of one nanowire. For nonideal contacts, the power is $P_{nonideal} = P_{ideal}/[(1 + (2\rho_c/\rho L_o))(1 + 2(\kappa/\kappa_c)(L_c/L_o))]$, where $r_c$ is the electrical resistivity of the contacts. For the new quantities in this equation not previously defined, we assume the following: $2\rho_c/\rho = 0.01$ and $\kappa/\kappa_c =$ various values as indicated. (d) Plot of the efficiency, $\phi$, for thermoelectric power generation for the devices shown in part a versus $L_o$ for three values of $\kappa/\kappa_c$. For nonideal contacts, $\phi = ((T_h - T_c)/T_h)\{(1 + 2(\kappa/\kappa_c)(L_c/L_o))^2[2 - 0.5((T_h - T_c)/T_h) + (4/ZT_h)((1 + 2\rho_c/\rho L_o)/[1 + 2(\kappa/\kappa_c)\ (L_c/L_o)])]\}^{-1}$, where all variables have already been defined except for $T_h$ and $T_c$. These are taken to be 325 and 300 K, respectively.[39]

$Te_3$ into the pores of a porous alumina membranes using a recipe for $Bi_2Te_3$ synthesis reported originally by Magri et al. involving the net reaction[32]

$$2Bi^{3+} + 3HTeO_2^{+} + 9H^{+} + 18e^{-} \rightarrow Bi_2Te_3 + 6H_2O \quad (2)$$

Nanowires with minimum diameters of 280, 40, and 50 nm, respectively, were obtained by these three research groups. Recently, some nontemplate synthesis methods have also been described: $Bi_2Se_3$ nanotubes, 5−10 nm in diameter and 80−120 nm in length, have been synthesized using a hydrothermal method by Liu and co-workers.[33] Two different solvothermal syntheses of $Bi_2Te_3$ nanorods have also been reported.[34,35]

Both synthesis and theory have emphasized the importance of achieving small nanowire diameters, but an engineering analysis of TE devices reveals that nanowires will also need to be extremely long in order for these devices to function efficiently. The importance of nanowire length has been neglected in all prior discussions of these materials, possibly because some performance metrics for "idealized" TE devices (Figure 1a) actually improve with decreasing nanowire length (e.g., Figure 1c). Min and Rowe,[36−39] however, have derived equations that allow performance metrics such as power, efficiency, and others to be calculated for realistic two-element Peltier devices (Figure 1b). The most important difference between an ideal device and a realistic device is the thermal contacts that in a real device have finite thickness and thermal conductivity. For a real device operated in power generation mode, the electrical power, $P_{nonideal}$, is given by[39]

$$P_{nonideal} = \frac{P_{ideal}}{(1 + 2\rho_c/\rho L_o)\left(1 + 2\frac{\kappa}{\kappa_c}\frac{L_c}{L_o}\right)} \quad (3)$$

where

$$P_{ideal} = \left(\frac{\alpha^2}{\rho}\right)\left(\frac{\Delta T^2}{2}\right)\left(\frac{A}{L_o}\right)$$

$\Delta$T is the temperature difference measured at the external surfaces of the ceramic layers, $A$ is the cross-sectional area of the two thermoelements, $\rho$ is the electrical resistivity of the nanowires with length $L_o$ and thermal conductivity $\kappa$, and $\rho_c$ is the electrical resistance of the contacts of total thickness (insulator + conductor), $L_c$, with a net thermal conductivity $\kappa_c$. When realistic values (Figure 1) are substituted for these parameters, the device power is maximized for nanowires that are 126 $\mu$m in length (for $\kappa/\kappa_c = 0.05$) or longer ($\kappa/\kappa_c > 0.05$), and $P$ falls rapidly with decreasing nanowire length below these optimum values. The plots of Figure 1c were calculated for nanowires with a diameter of 100 nm, but the optimum nanowire lengths, indicated by the arrows, are identical across the diameter range from 1 to 100 nm.

(20) Martin, C. R. *Science* **1994**, *266*, 1961.
(21) Martin, C. R. *Chem. Mater.* **1996**, *8*, 1739.
(22) Hulteen, J. C.; Martin, C. R. *J. Mater. Chem.* **1997**, *7*, 1075.
(23) Sapp, S. A.; Lakshmi, B. B.; Martin, C. R. *Adv. Mater.* **1999**, *11*, 402.
(24) Sander, M. S.; Prieto, A. L.; Gronsky, R.; Sands, T.; Stacy, A. M. *Adv. Mater.* **2002**, *14*, 665.
(25) Prieto, A. L.; Sander, M. S.; Martin-Gonzalez, M. S.; Gronsky, R.; Sands, T.; Stacy, A. M. *J. Am. Chem. Soc.* **2001**, *123*, 7160.
(26) Sander, M. S.; Gronsky, R.; Sands, T.; Stacy, A. M. *Chem. Mater.* **2003**, *15*, 335.
(27) Martin-Gonzalez, M. S.; Prieto, A. L.; Gronsky, R.; Sands, T.; Stacy, A. M. *J. Electrochem. Soc.* **2002**, *149*, C546.
(28) Prieto, A. L.; Martin-Gonzalez, M.; Keyani, J.; Gronsky, R.; Sands, T.; Stacy, A. M. *J. Am. Chem. Soc.* **2003**, *125*, 2388.
(29) Martin-Gonzalez, M.; Prieto, A. L.; Knox, M. S.; Gronsky, R.; Sands, T.; Stacy, A. M. *Chem. Mater.* **2003**, *15*, 1676.
(30) Wang, W.; Huang, Q. H.; Jia, F. L.; Zhu, J. *J. Appl. Phys.* **2004**, *96*, 615.
(31) Wang, W.; Zhang, W. L.; Wang, H.; Tao, S.; Zhang, J. Z. *J. Inorg. Mater.* **2004**, *19*, 127.
(32) Magri, P.; Boulanger, C.; Lecuire, J. M. *J. Mater. Chem.* **1996**, *6*, 773.
(33) Cui, H. M.; Liu, H.; Li, X.; Wang, J. Y.; Han, F.; Zhang, X. D.; Boughton, R. I. *J. Solid State Chem.* **2004**, *177*, 4001.
(34) Deng, Y.; Nan, C. W.; Wei, G. D.; Guo, L.; Lin, Y. H. *Chem. Phys. Lett.* **2003**, *374*, 410.
(35) Purkayastha, A.; Lupo, F.; Kim, S.; Borca-Tasciuc, T.; Ramanath, G. *Adv. Mater.* **2006**, *18*, 496.
(36) Min, G. O.; Rowe, D. M. *J. Power Sources* **1992**, *38*, 253.
(37) Rowe, D. M.; Min, G. *IEE Proc.: Sci., Meas. Technol.* **1996**, *143*, 351.
(38) Min, G.; Rowe, D. M. *Energy Convers. Manage.* **2000**, *41*, 163.
(39) Rowe, D. M. *CRC Handbook of Thermoelectrics*; CRC Press: London, 1995.

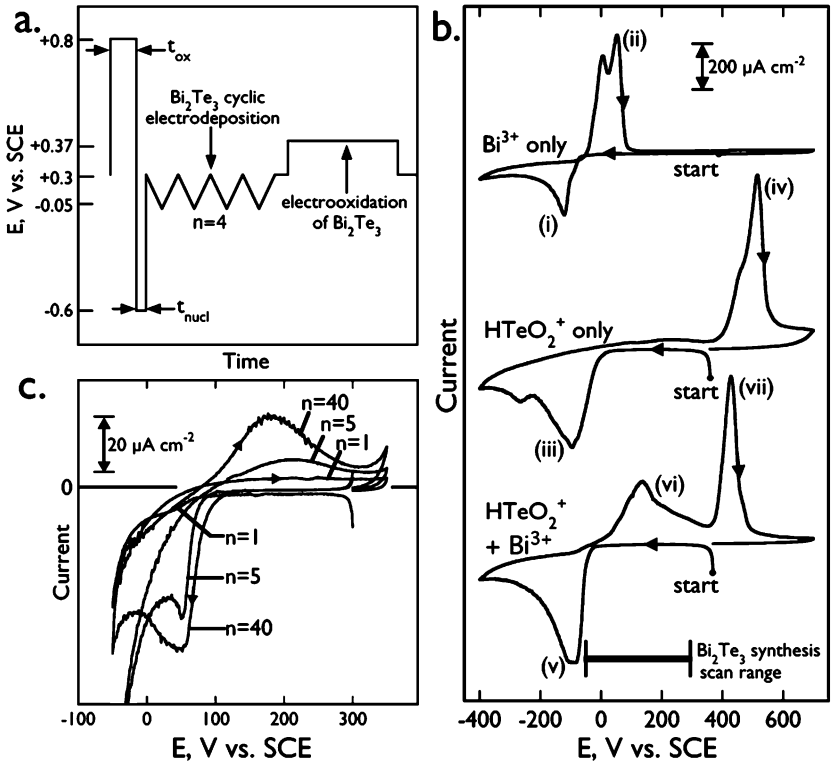


**Figure 2.** (a) Potential program used for the synthesis and electrooxidation of $Bi_2Te_3$ nanowires on HOPG electrodes. The electrodeposition of $Bi_2Te_3$ nanowires involves three steps: (1) potentiostatic oxidation of step edges on the HOPG surface at $E_{ox} = 0.80$ V vs SCE for a time, $t_{ox} = 5$ s; (2) potentiostatic nucleation of $Bi_2Te_3$ at $E_{nucl} = -0.75$ V for $t_{nucl} = 5$ ms; and (3) cyclic electrodeposition of stoichiometric $Bi_2Te_3$ involving $n$ potential cycles at 20 mV s$^{-1}$ between a positive limit of $E_{(+)}$ (+0.35 V) and a negative limit of $E_{(-)}$ (−0.05 V). Electrooxidation adds a fourth step: potentiostatic oxidation at +0.37 V. (b) Cyclic voltammograms at 20 mV s$^{-1}$ for an HOPG electrode in contact with three different aqueous plating solutions: (top) 1.5 mM $Bi(NO_3)_3$ in 1 M $HNO_3$; (middle) 1.0 mM TeO in 1 M $HNO_3$; and (bottom) 1.5 mM $Bi(NO_3)_3$ and 1.0 mM TeO in 1 M $HNO_3$. (c) CVs acquired during the growth of $Bi_2Te_3$ nanowires using cyclic electrodeposition/stripping. The CV is shown at scans 1, 5, and 40 as indicated.

The thermoelectric efficiency, $\phi$, for the same devices increases monotonically with nanowire length, as shown in Figure 1d. These calculations lead immediately to the conclusion that nanowires longer than any synthesized to date will be required for device applications.

Recently, we described a new technique for the synthesis of arrays of hundreds of $Bi_2Te_3$ nanowires that are more than 100 $\mu$m in length.[40] $Bi_2Te_3$ nanowires were obtained by coupling a cyclic electrodeposition/stripping method for synthesizing $Bi_2Te_3$ with electrochemical step edge decoration[41−47] at HOPG step edges. Our initial attempts to characterize these materials by XRD and X-ray fluorescence electron microprobe analysis are consistent with the formation of rhombohedral $Bi_2Te_3$ (JCPDS 15-0863) having approximately correct Bi/Te stoichiometry. These nanowires had diameters in the range of 100 to 300 nm; however, by adding an electrooxidation step, the diameter of 130 nm wires was reduced to ∼30 nm.[48] This full paper provides a complete description of our synthesis procedure, the procedure for electrooxidation, and a more comprehensive assessment of the composition of these nanowires derived from X-ray photoelectron spectroscopy (XPS), electron microscopy, and electron and X-ray diffraction analyses of these materials. We also disclose the results of our initial attempts to measure *ZT* for ensembles of these nanowires.

## II. Experimental Methods and Materials

**$Bi_2Te_3$ Nanowire Synthesis.** The electrochemical deposition of $Bi_2Te_3$ was carried out in a 50 mL, one compartment, glass and Teflon three-electrode cell. The plating solution consisted of 1.5 mM bismuth(III) nitrate pentahydrate (Aldrich, 99.999%) and 1 mM tellurium oxide (Aldrich, 99.999%) in 1 M nitric acid prepared according to the published procedure.[32] This plating solution was prepared using Nanopure water ($\rho > 17.6$ MΩ) and was purged with $N_2$ prior to each experiment. A saturated calomel reference electrode (SCE) and a 2 cm$^2$ Pt foil counter electrode were also employed. The working electrode for these electrodeposition experiments was the basal plane surface of ZYA- or ZYB-grade HOPG crystals from GE Advanced Ceramics Inc. (Cleveland, OH). The basal plane surface was cleaved with adhesive tape prior to use, and a circular area of 0.2 cm$^2$ was exposed, using an O-ring, to this plating solution. The depositions were carried out on an EG&G 273A potentiostat/galvanostat.

Nanowires were prepared using the potential program shown in Figure 2a. This program accomplished the following four steps in succession: (1) oxidation of the HOPG step edges at 0.80 V versus SCE for 5 s; (2) nucleation of $Bi_2Te_3$ and elemental bismuth at $E_{nucl} = -0.75$ versus SCE for 5 ms; (3) growth of $Bi_2Te_3$ nuclei and removal of excess elemental bismuth by cyclic electrodeposition−stripping using potential limits of $E_{(-)} = -0.05$ V and $E_{(+)} = +0.350$ V versus SCE at a rate of 20 mV s$^{-1}$ for a varying number of scans ranging from 10 to 90; and (4) electrooxidation of the $Bi_2Te_3$

(40) Menke, E. J.; Li, Q.; Penner, R. M. *Nano Lett.* **2004**, *4*, 2009.
(41) Zach, M. P.; Ng, K. H.; Penner, R. M. *Science* **2000**, *290*, 2120.
(42) Favier, F.; Walter, E. C.; Zach, M. P.; Benter, T.; Penner, R. M. *Science* **2001**, *293*, 2227.
(43) Walter, E. C.; Favier, F.; Penner, R. M. *Anal. Chem.* **2002**, *74*, 1546.
(44) Penner, R. M. *J. Phys. Chem. B* **2002**, *106*, 3339.
(45) Walter, E. C.; Murray, B. J.; Favier, F.; Kaltenpoth, G.; Grunze, M.; Penner, R. M. *J. Phys. Chem. B* **2002**, *106*, 11407.
(46) Walter, E. C.; Murray, B. J.; Favier, F.; Penner, R. M. *Adv. Mater.* **2003**, *15*, 396.
(47) Li, Q.; Newberg, J. T.; Walter, E. C.; Hemminger, J. C.; Penner, R. M. *Nano Lett.* **2004**, *4*, 277.
(48) Thompson, M. A.; Menke, E. J.; Martens, C. C.; Penner, R. M. *J. Phys. Chem. B* **2006**, *110*, 36.

nanowires at +0.37 V versus SCE for times ranging from 0 to 800 s, which allowed for a reduction in diameter down to 30 nm. The HOPG working electrode was then removed from solution, rinsed with Nanopure water, and air dried prior to characterization.

**Electron Microscopy.** Scanning electron microscopy (SEM) images and energy-dispersive X-ray fluorescence (EDX) analysis were acquired on a Philips model XL-30FEG operating at 20 kV. Samples were mounted on aluminum SEM stubs using adhesive carbon dots from Ted Pella. Transmission electron microscopy (TEM) and selected-area electron diffraction (SAED) data were acquired on a Philips model CM20 operating at 200 kV. Samples for TEM and SAED were prepared by cleaving a thin layer of graphite from the basal plane of HOPG that nanowires had been deposited onto. This piece of graphite was then placed on a gold TEM grid (Ted Pella) and was thin enough near the edges to allow for imaging and electron diffraction.

**Powder X-ray Diffraction (XRD).** XRD patterns were acquired on a Siemens D5000 diffractometer using a Cu Kα X-ray source operating at 40 keV and 30 mA. An angle of incidence of 22.5° with respect to the sample was employed. The detector scanned from $2\theta = 25°$ to $2\theta = 70°$, with a step size of 0.02° and 3 s per step, for a total time of approximately 2 h per spectra. The peak positions were calibrated using the HOPG crystal as an internal reference.

**X-ray Photoelectron Spectroscopy.** XPS measurements were performed with an Escalab MKII (VG Scientific) surface analysis system. The system is a multichamber ultrahigh vacuum system equipped with a twin anode X-ray source (Mg/Al) and a 150 mm hemispherical electron energy analyzer. Spectra presented here were obtained using Al Kα X-rays (1486.7 eV). During these experiments, the base pressure in the spectroscopy chamber was $1 \times 10^{-9}$ Torr. The experiments were carried out with the energy analyzer in constant analyzer energy mode and at a pass energy of 20 eV. The peak positions were calibrated using the C (1s) peak of the HOPG substrate at 284.5 eV as a reference.[49]

**Device Preparation and *ZT* Measurement.** $Bi_2Te_3$ nanowires on HOPG were embedded in a cyanoacrylate film and transferred to a glass microscope slide as previously described.[43] A custom shadow mask (Photo Sciences, Inc.) was then positioned over the nanowire array using an optical microscope, and approximately 100 nm of nickel was thermally evaporated onto the nanowire array through the shadow mask to form four electrical contacts. Between 10 and 100 nanowires were typically continuous with all four contacts, but the exact number of electrically continuous nanowires present in each device was not known.

*ZT* was measured using the method described by Harmon.[50] A constant current of a few microamps was run through the two outer nickel contacts until a constant voltage at the inner contacts was observed. Then, at time $t = 0$, the current was switched off while the voltage drop across the inner electrodes was measured using a National Instruments PCI-6111 DAQ board in conjunction with a Texas Instruments INA-111 high-speed FET instrumentation amplifier, providing a gain of 2 and impedance matching between the nanowires and the DAQ board. The voltage−time transient for each device was measured 100 times, and these transients were then averaged to provide the data presented in Figure 8d. Two parameters were extracted from averaged transients: $V_{total}$ and $V_0$, as shown schematically in Figure 8c. *ZT* was calculated as[50]

$$ZT = \frac{V_0}{V_{total} - V_0} \tag{4}$$

## III. Results and Discussion

**A. $Bi_2Te_3$ Electrodeposition by Cyclic Electrodeposition/Stripping.** The potential program for synthesizing $Bi_2Te_3$ nanowires (Figure 2a) involved four steps: First, the HOPG surface was oxidized at +0.8 V versus SCE for 5 s. This treatment increased the nucleation density at step edges, but the graphite basal plane is not attacked at this potential. Second, a nucleation pulse of −0.75 V × 5 ms was applied. This pulse produced nanoparticles of $Bi_2Te_3$ and elemental bismuth both at step edges and also on atomically smooth regions of the HOPG basal plane. Third, these nuclei were grown using a cyclic electrodeposition/stripping scheme that involved scanning between a negative potential limit of $E(-) = -0.05$ V and a positive limit of $E(+) = +0.350$ V at a rate of 20 mV $s^{-1}$. Between 10 and 90 synthesis cycles were used to build up nanowires of $Bi_2Te_3$ with diameters between 100 and 330 nm. Finally, in selected instances, nanowires were electrooxidized at +0.37 V in order to reduce their diameter from 100−130 nm to 30 nm. All four of these steps were carried out in rapid succession while these nanowires were immersed in an aqueous solution of 1.5 mM $Bi^{3+}$ and 1 mM $HTeO_2^+$ in 1.0 M nitric acid at room temperature. The composition of this solution is intentionally weighted toward bismuth to avoid the deposition of excess tellurium because, as discussed in greater

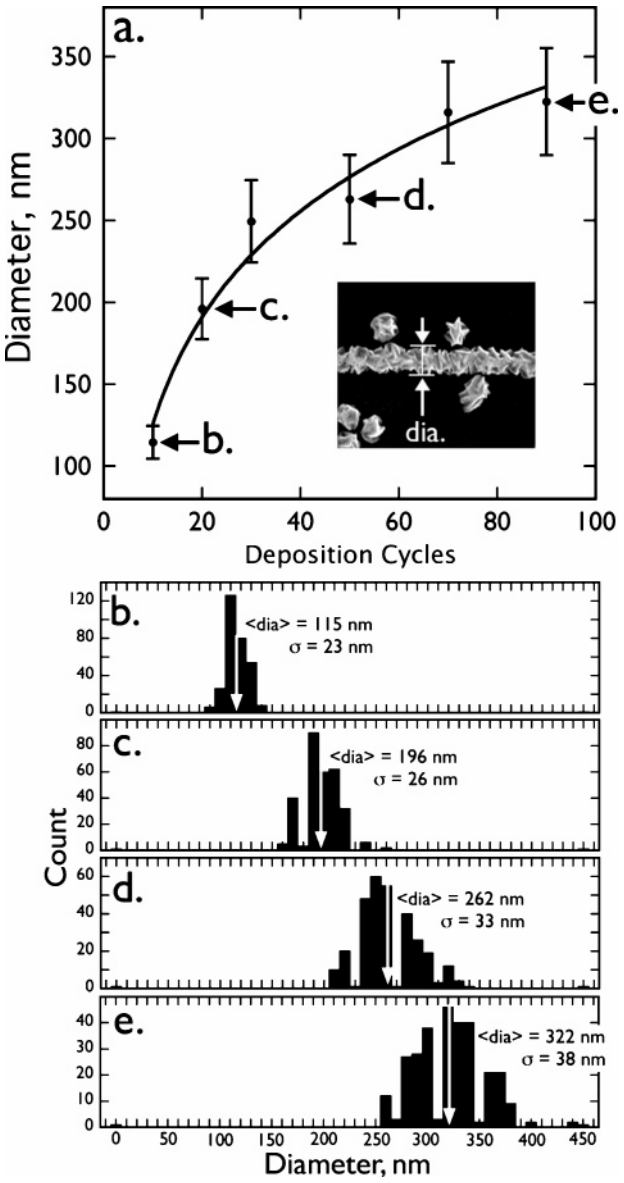


**Figure 3.** (a) Plot of nanowire diameter as a function of the number of electrodeposition cycles. (b−e) Histograms of the nanowire diameter for samples prepared using 10, 20, 50, and 90 electrodeposition/stripping scans.

(49) Moulder, J. F.; Stickle, W. F.; Sobol, P. E.; Bomben, K. D. *Handbook of X-ray Photoelectron Spectroscopy*; Perkin-Elmer, Physical Electronics Division: Eden Prarie, MN, 1992.

(50) Harman, T. C.; Cahn, J. H.; Logan, M. J. *J. Appl. Phys.* **1959**, *30*, 1351.

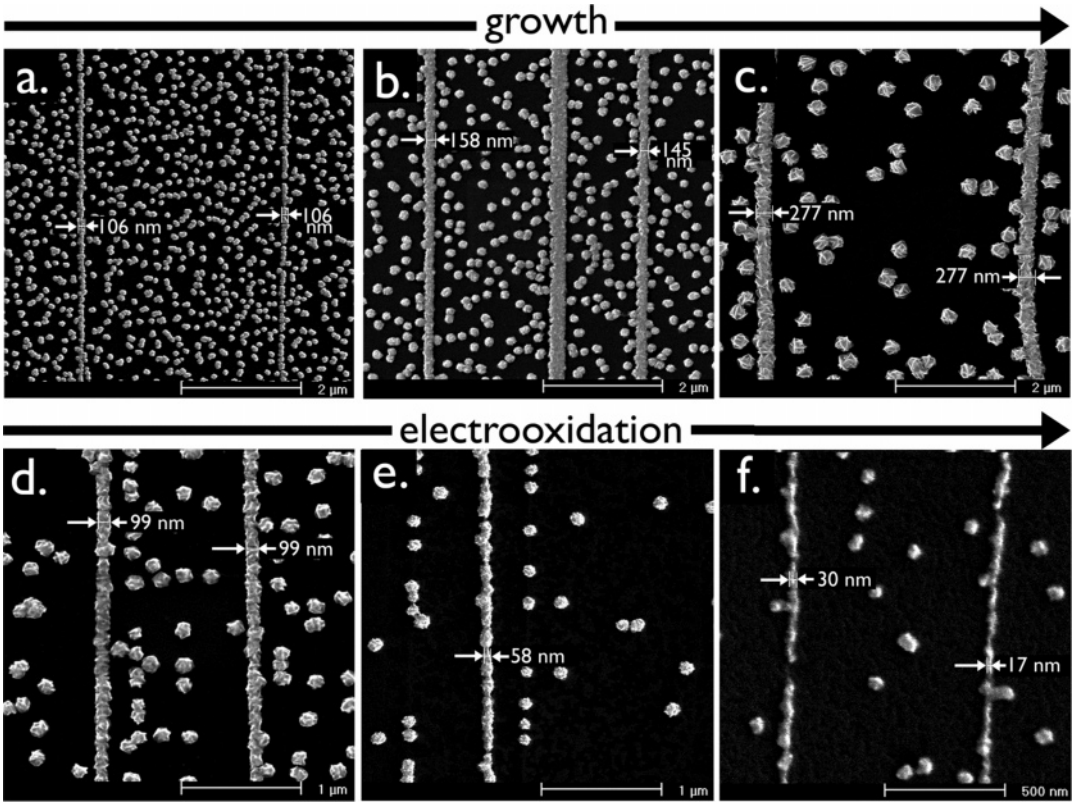


**Figure 4.** (a−c) Scanning electron micrographs (SEMs) of three $Bi_2Te_3$ nanowire samples prepared using 10, 20, and 50 electrodeposition/stripping scans. (d−f) SEMs of three $Bi_2Te_3$ nanowire samples prepared by electrooxidation at +0.37 V for (d) 200, (e) 600, and (f) 800 s. The initial diameter of these nanowires before oxidation was 130 nm + 15 nm.

detail below, elemental tellurium is not stripped within the potential window (−0.05 to +0.35 V) used for $Bi_2Te_3$ synthesis.

The cyclic voltammograms (CVs) for the synthesis solution employed in this work are shown in Figure 2b. Also shown are CVs for solutions in which just one of the reactants, either $HTeO_2^+$ or $Bi^{3+}$, was present. On the basis of prior work by Stacy and the EDX analysis of the electrodeposited material, the principle voltammetric peaks in these cyclic voltammograms are assigned as follows:

$$\text{peaks i and ii } Bi^{3+} + 3e^- \rightarrow Bi^0 \quad (5)$$

and the reverse reaction

$$\text{peaks iii and iv } HTeO_2^+ + 3H^+ + 4e^- \rightarrow Te + 2H_2O \quad (6)$$

and the reverse reaction

$$\text{peak vi } Bi^0 \rightarrow Bi^{3+} + 3e^- \quad (7)$$

$$\text{peaks v and vii } 2Bi^{3+} + 3HTeO_2^+ + 9H^+ + 18e^- \rightarrow Bi_2Te_3 + 6H_2O \quad (8)$$

and the reverse reaction

On the basis of these assignments, it is immediately clear why the cyclic electrodeposition−stripping strategy is essential for the synthesis of stoichiometric $Bi_2Te_3$ at HOPG electrodes: At any voltage negative enough to deposit $Bi_2Te_3$ (Figure 2b, bottom), elemental bismuth and tellurium are also deposited (Figure 2b top and middle). In a comprehensive study of $Bi_2Te_3$ electrodeposition in nitric acid at platinum electrodes, Stacy et al.[27] proposed that the synthesis of $Bi_2Te_3$ at low overpotentials occurs in two steps involving the electrodeposition of elemental tellurium according to reaction 6, followed by the reaction of tellurium with $Bi^{3+}$ to form $Be_2Te_3$:

$$3Te + 2Bi^{3+} + 6e^- \rightarrow Bi_2Te_3 \quad (9)$$

Reactions 6 and 9 sum to give net synthesis reaction 2 for $Bi_2Te_3$. Stacy and co-workers believe a second mechanism, involving $H_2Te$ as an intermediate, operates in parallel to produce $Bi_2Te_3$,[27] but at potentials that are 500−600 mV more negative. Here, we have selected as the negative limit for our synthesis scans the most positive potential capable of producing $Bi_2Te_3$ (−0.05 V vs SCE) because an extremely low rate of $Bi_2Te_3$ growth is required to avoid the progressive nucleation of this material on the HOPG terraces (see below). Thus, our synthesis conditions should favor the first of these two mechanisms. The nucleation of tellurium (reaction) that occurs at −0.05 V has a significant overpotential associated with it, even though the nucleation pulse applied first produces nuclei on the HOPG surface prior to scanning. This nucleation overpotential is decreased as increasing quantities of $Bi_2Te_3$ are deposited, as seen by the positive shift in the onset of reduction in Figure 2c.

Analysis by scanning electron microscopy (SEM) reveals that the coalescence of $Bi_2Te_3$ nanoparticles into polycrystalline nanowires occurs at a nanowire diameter of ∼100 nm, after approximately 10 electrodeposition/stripping scans (Figure 3a). Typical SEM images of such nanowires are shown in Figure 4a. Larger nanowires, up to 300 nm in diameter, are obtained by increasing the number of synthesis scans (Figures 3a and 4b and c). These nanowires are narrowly distributed in diameter (Figure 3b) and are more than 100 $\mu$m in length. In addition to nanowires, many $Bi_2Te_3$ nanoparticles are electrodeposited on the terraces present between step edges (Figure 4a−c). The growth of such

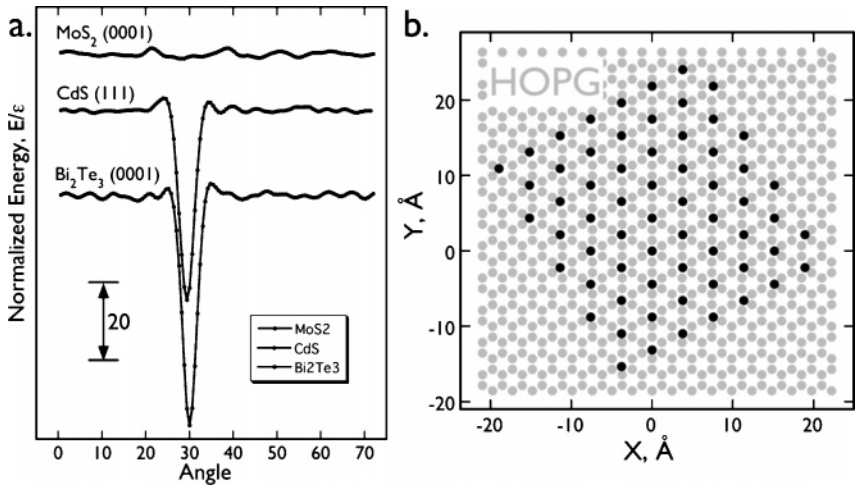


**Figure 5.** (a) Plot of the normalized energy ($E/e_o$) vs angle for two-layer-thick islands of $Bi_2Te_3$, $MoS_2$, and wurtzite CdS calculated using a Lennard-Jones 6−12 potential with well depth of $\epsilon_o$. These islands were square, ~20 Å × 20 Å, and consisted of 124 atoms partitioned into two layers of equal size. The graphite surface also consisted of two layers each containing 941 atoms. (b) Atom positions on the graphite surface corresponding to the orientation that yielded the minimum energy for $Bi_2Te_3$ seen in part a.

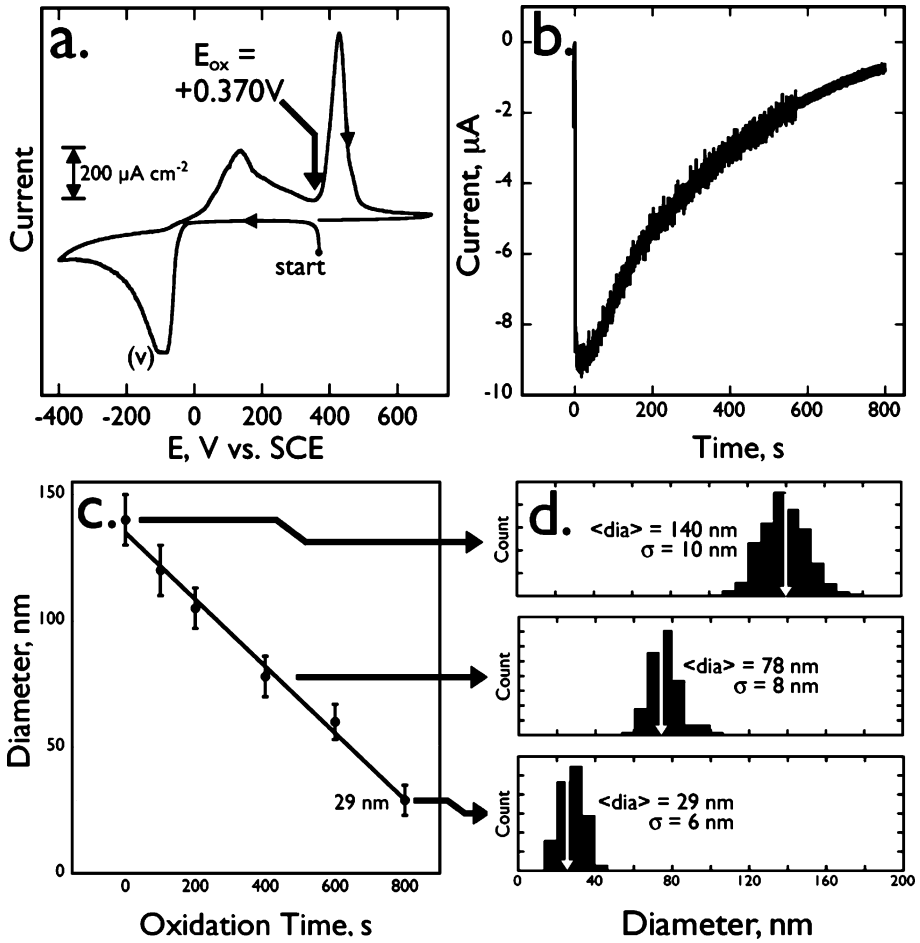


**Figure 6.** (a) Cyclic voltammogram at 20 mV $s^{-1}$ in aqueous 1.5 mM $Bi(NO_3)_3$ and 1.0 mM TeO in 1 M $HNO_3$ showing the potential employed for the kinetically controlled electrooxidation of $Bi_2Te_3$ nanowires. (b) Current vs time transient for the electrooxidation of $Bi_2Te_3$ nanowires that had an initial diameter of 140 nm. (c) Plot of mean nanowire diameter vs electrooxidation time for six oxidation times. (d) Diameter histograms for three samples of $Bi_2Te_3$ nanowires. The top histogram was representative of the diameter distribution before etching (top) and after electrooxidation for 400 s (middle) and 800 s (bottom).

nanoparticles is always a byproduct of nanowire growth, but the number density of these particles is higher here than is typically seen, suggesting that these $Bi_2Te_3$ nanoparticles nucleate readily on the graphite basal plane. One possible reason for this is the a spacing for rhombohedral $Bi_2Te_3$ of 4.385 Å, which almost coincides with the 2*d*[100] spacing for HOPG of 4.2772 Å, a mismatch of just 2.5%. The resulting coincidence between these lattices, shown in Figure 5b, leads to a pronounced minimum in the energy calculated for a small $Bi_2Te_3$ island at an azimuthal angle of 30° (Figure 5a). Exactly this same effect leads to the epitaxial electrodeposition of a high density of CdS islands on HOPG surfaces.[51]

**B. Shrinking $Bi_2Te_3$ Nanowires by Kinetically Controlled Electrooxidation.** $Bi_2Te_3$ nanowires of 100 nm diameter are at least an order of magnitude too large to show the beneficial thermal transport properties projected for one-dimensional materials. As already indicated, $Bi_2Te_3$ is oxidized to soluble products in a well-defined voltammetric process (peak vii in Figure 2b):

$$Bi_2Te_3 + 6H_2O \rightarrow 2Bi^{3+} + 3HTeO_2^{+} + 9H^{+} + 18e^{-} \quad (10)$$

Thus, one method for producing smaller nanowires is to apply this electrooxidation reaction to ~100-nm-diameter $Bi_2Te_3$ nanowires. A study of this electrooxidation strategy that included the metals antimony and gold[48] revealed that nanowires of these metals remained continuous during oxidation only when the oxidation rate was extremely low. In this kinetically controlled limit, the current density on the surface of the nanowire is expected to be constant, and the total electrooxidation current density measured during the oxidation process decreases with time as the surface area of these nanowires is diminished, as shown in Figure 6b. This oxidation current transient cannot be quantitatively modeled because the oxidation of both nanoparticles and nanowires contributes to this current. The nanowire radius is predicted to decrease in direct proportion to the oxidation time, according to[48]

$$r(t) = r_{o2} - \frac{j_{ox} t_{ox} V_m}{nF} \quad (11)$$

Equation 11 predicts that d*r*/d*t* is radius-independent and that nanowires retain their initial roughness as they become narrower. We found empirically that this limit was achieved for $Bi_2Te_3$ oxidation at a potential of +0.37 V (Figure 6a), and in our investigation of this process, we first deposited SEM images of $Bi_2Te_3$ nanowires that were 130 nm in diameter and then electrooxidized them at +0.37 V for various durations. Typical SEM images obtained after 200, 600, and 800 s of oxidation (Figure 4d−f) show that the oxidized nanowires show few breaks even after shrinking to a diameter of 30 nm. The time dependence of the nanowire diameter is linear with oxidation time, just as predicted for a kinetically controlled process. Surprisingly, the diameter distribution of these nanowires (Figure 6d) actually narrows slightly during oxidation, an effect that is not anticipated on the basis of eq 11. Does the removal of $Bi_2Te_3$ by electrooxidation perturb the composition of the $Bi_2Te_3$ that remains on the HOPG surface? This issue is addressed by the XPS study presented in section III.E below.

**C. Energy-Dispersive X-ray (EDX) Microanalysis, X-ray Diffraction (XRD), and Electron Diffraction Analyses.** Energy-dispersive X-ray microanalysis (EDX) provides a means for estimating the elemental composition of materials within a suitably equipped SEM. The probe depth of EDX is approximately 2 $\mu$m for 20 keV electrons so for the ~200-nm-diameter nanowires examined here, EDX elemental analysis will report on the bulk composition of the nanowires. EDX elemental analysis of $Bi_2Te_3$ nanowires (data not shown) produced a Bi−Te atomic ratio of 2:3.4, slightly lower than the 2:3 stoichiometry of this compound would predict but in agreement with the composition predicted from the Bi−Te phase diagram.[52]

X-ray diffraction analyses in prior papers[24−26,28−31] have demonstrated that rhombohedral $Bi_2Te_3$ (JCPDS 15-0863) is produced using conditions of solution composition and pH similar to those that we are employing here, just as originally reported by Magri et al.[32] Because of the small quantities of material present on our surfaces, we were not able to acquire XRD patterns for nanowires smaller than 500 nm. Shown in Figure 7a are patterns obtained for $Bi_2Te_3$ depositions of 1, 5, and 10 h. The 1 h deposition produced 500-nm-diameter nanowires whereas the 5 and 10 h depositions produced $Bi_2Te_3$ films. These samples produced relatively strong diffraction patterns that assisted us in the confirmation and assignment of low signal-to-noise peaks in the pattern for 500-nm-diameter wires (Figure 7a). All of the peaks seen in these patterns were assignable either to rhombohedral $Bi_2Te_3$ (JCPDS 15-0863) or to the graphite substrate. However, diffractions corresponding to out-of-plane periodicities, including 110, 205, 116, and 125, were more intense than expected for isotropically distributed crystallites relative to 015, and in-plane periodicities 1010 and 1115 were weaker than expected. Because XRD is most sensitive to the out-of-plane periodicities,

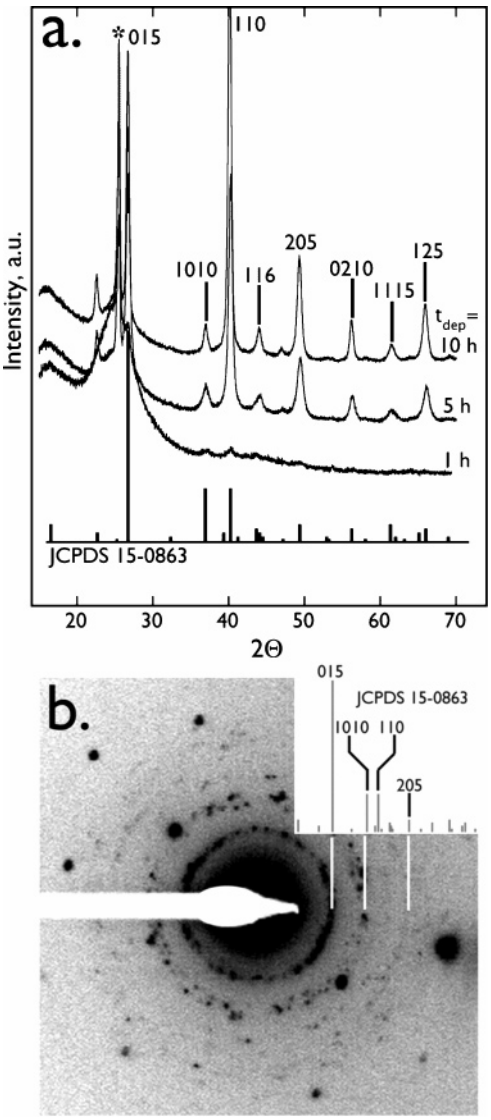


**Figure 7.** (a) Powder X-ray diffraction for three $Bi_2Te_3$ samples prepared by cyclic electrodeposition/stripping for 1, 5, and 10 h. The 5 and 10 h samples were continuous films of $Bi_2Te_3$ whereas the 1 h sample consisted of wires with a mean diameter of approximately 500 nm. (b) Selected-area electron diffraction pattern for a $Bi_2Te_3$ nanowire. White lines mark the expected position of diffractions for rhombohedral $Bi_2Te_3$, JCPDS card 15-0863, as shown. Diffractions from the crystalline graphite substrate are also indicated.

(51) Gorer, S.; Ganske, J. A.; Hemminger, J. C.; Penner, R. M. *J. Am. Chem. Soc.* **1998**, *120*, 9584.

(52) Okamoto, H.; Tanner, L. E. *Bi−Te (Bismuth−Tellurium) Phase Diagram*; ASM: 1986.

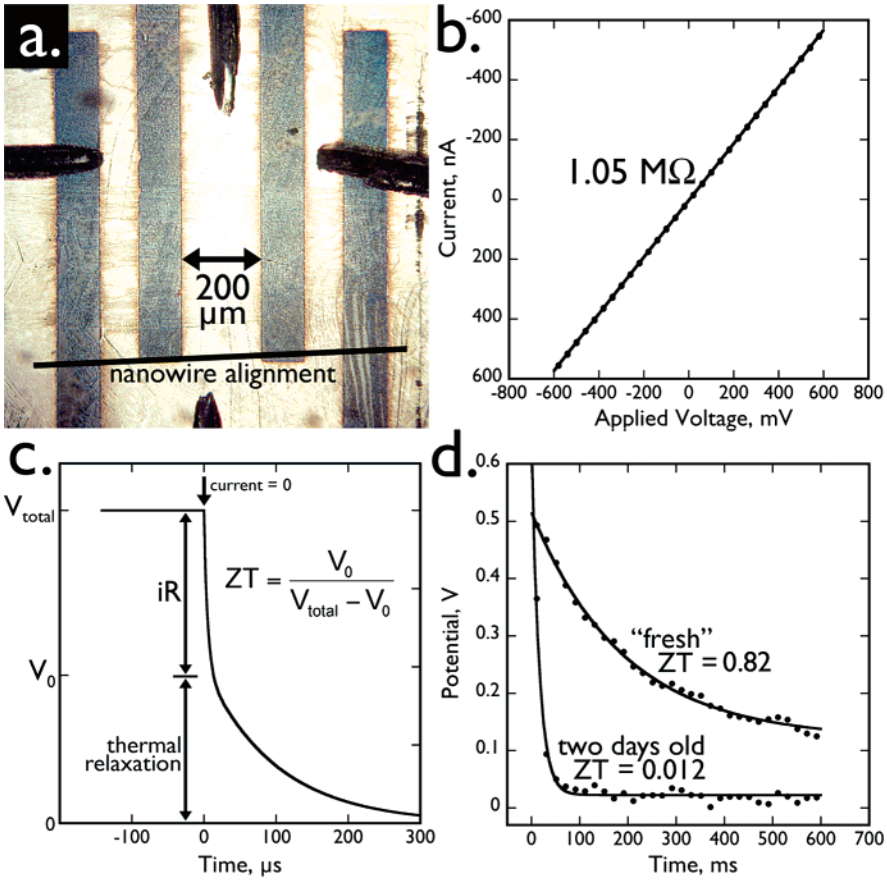


**Figure 8.** (a) Photograph of four evaporated nickel contacts (gray) used for the evaluation of *ZT* for ensembles of $Bi_2Te_3$ nanowires that were transferred to cyanoacrylate-coated glass microscope slides. The alignment of these nanowires on the surface is indicated by the black line at the bottom. Only nanowires contacting the outermost nickel contacts, separated by 600 $\mu$m, contributed to the measured electrical responses. (b) Either nickel or gold electrical contacts produced by evaporation yielded ohmic current−voltage behavior, as shown here for $Bi_2Te_3$ nanowires with a diameter of ∼130 nm. (c) Schematic diagram of an ideal voltage vs time transient for a thermoelectric material showing the two quantities, $V_0$ and $V_{total}$, required for the calculation of *ZT* using eq 4. (d) Potential vs time transients, averaged for 100 trials, for 1 particular sample among 40 that produced the highest *ZT* value of 0.82. Shown are two transients for the same sample of $Bi_2Te_3$ nanowires. The first, labeled "fresh", is the response measured after approximately 1 h of air exposure, and the second, labeled "2 days old", is the response seen after 2 days of air exposure.

this skewing means that a crystallographically preferred growth direction exists along 110. This preferred orientation is likely caused by the near-perfect lattice match of $Bi_2Te_3$ to the graphite lattice, as already described in section III.A. Evidence for this "texturing" is also seen in the selected-area electron diffraction (SAED) pattern that, in contrast to XRD, is most sensitive to in-plane periodicities. In the SAED pattern of Figure 7b, the 205 reflection is absent (the diffraction spot shown there is derived from graphite), but 015 is observed and is consistent with hexagonal $Bi_2Te_3$. A crucial question that is not resolved by XRD, however, is the completeness of reaction 9 and the extent to which reaction 7 produces elemental bismuth that remains unreacted during the electrodeposition of $Bi_2Te_3$. The point is that either elemental Te or Bi or their oxides may be present and undetected by XRD either within the interstices of crystalline $Bi_2Te_3$ nanowires or more likely at the surfaces of these nanowires. We believe the presence of surface impurities is at the root of the irreproducibility seen for our measurements of *ZT* (section III.D), and the identification of these impurities provides the motivation for the XPS study (section III.E).

**D. Preliminary Measurements of *ZT*.** The widely accepted[39] method of Harman[50] was employed to measured *ZT* for 40 different ensembles of 200-nm-diameter $Bi_2Te_3$ nanowires prepared using 20 electrodeposition/stripping cycles. These nanowires were not subjected to electrooxidation to minimize the formation of surface oxides. (See the discussion in section III.E.) After transferring these nanowire ensembles to a cyanoacrylate-coated glass microscope slide, four nickel contacts were evaporated as seen in Figure 8a. The inner contacts were spaced by 200 $\mu$m, and the outer contacts, by 600 $\mu$m. Thus the shortest nanowires contributing to *ZT* in this device were at least 600 $\mu$m in total length. Evaporated nickel produced ohmic contacts to these nanowires as evidenced by the fact that ohmic current−voltage curves were reproducibly obtained for $Bi_2Te_3$ nanowire ensembles (Figure 8b). It should be noted that nanowires within this device are not well isolated thermally. Instead, they are strongly thermally coupled to a glass surface through the cyanoacrylate layer. The resulting parasitic thermal losses to the glass surface will depress the measured value of *ZT*.

*ZT* was measured by flowing a constant current of a few microamperes through the outer two contacts until a time-invariant voltage, $V_{total}$, was measured at the inner two contacts. The current was then interrupted, and the resulting voltage−time transient was measured using suitable electronics as described in the Experimental Section. This transient (Figure 8d) consisted of a rapid (1−5 $\mu$s) voltage drop equal to $V_0$ caused by the ohmic resistance of the nanowires and a slower decay of the remaining thermal voltage associated with the relaxation of the temperature gradient produced within the nanowires. *ZT* was then calculated using eq 4.[50]

We found two distinct behaviors for the nanowire ensembles that we measured using this method: most (37 out of 40) nanowire

samples produced no measurable thermal voltage ($V_0 \approx 0$ V). We can place an upper limit on the *ZT* produced by these samples of 0.05. One sample produced a *ZT* of 0.2, one a *ZT* of 0.72, and one a *ZT* of 0.82. Because these higher-*ZT* values represent the mean obtained for 100 replicate current interrupt measurements, we deem them to be reliable although these nonzero *ZT* values were seen in just 5% of the nanowire samples that we measured. Especially in view of the good material characterization metrics that we have already presented above, the origin of this irreproducibility in the measurement of *ZT* was initially puzzling to us. We measured many of these samples multiple times over a period of days, but devices that showed a *ZT* of near zero did not subsequently produce a measurable *ZT*. However, the sample that produced $ZT = 0.82$ showed a much different response, and a lower *ZT*, after 2 days of air exposure (Figure 8d). This observation, coupled with the conclusions derived from the XPS analysis reported below, suggests that the formation of a surface oxide may be responsible both for the absence of a measurable *ZT* at most nanowire samples and for the observed decay in *ZT* seen in Figure 8d. It should be noted that $ZT = 0.82$ is close to the maximum value measured for $Bi_2Te_3$ pellet devices at room temperature.[39]

**E. X-ray Photoelectron Spectroscopy.** The chemical state of the nanowire surface is a critical issue for thermoelectric applications because low-resistance electrical contacts to the surface of these nanowires must be prepared by metal evaporation. Here, X-ray photoelectron spectroscopy (XPS) was used to probe the chemical composition of the outermost 1−5 nm (depending on the photoelectron kinetic energy) of the nanowire surface. Three samples of $Bi_2Te_3$ nanowires were examined by XPS: freshly deposited nanowires prepared using 20 electrodeposition/stripping scans and nanowires electrooxidized at +0.37 V for 400 and 800 s. Each of these three samples was examined within an hour or so after synthesis to try to minimize the surface oxidation and then again after 1 week of exposure to laboratory air. Our results are summarized in Table 1.

The photoelectron spectra for both bismuth and tellurium are shown in Figures 9a and c and 9b and d, respectively. The bismuth spectra reveal two sets of doublets, one at binding energies of 156.7 and 162.0 eV and the other at binding energies of 158.2 and 163.5 eV, corresponding to the bismuth $4f_{7/2}$ and $4f_{5/2}$ spin states of two different chemical states. The tellurium spectra also contain two sets of doublets, one with binding energies of 572.4 and 582.8 eV and the other with binding energies of 575.6 and 586.0 eV, corresponding to the tellurium $3d_{5/2}$ and $3d_{3/2}$ spin states of two chemically different states. In the analysis that follows, we focus attention on the photoelectron peaks of bismuth $4f_{7/2}$ and tellurium $3d_{5/2}$, and we tabulate these chemical shifts for comparison with literature values in Table 1.

Parts a and b of Figure 9 show spectra for freshly synthesized $Bi_2Te_3$ nanowires after approximately 1 h of air exposure. In all spectra, the lower-binding-energy peak is more intense than the higher-binding-energy peak. As shown in Table 1, the chemical shifts for the lower-binding-energy peaks at 156.7 and 572.4 eV for bismuth $4f_{7/2}$ and tellurium $3d_{5/2}$, respectively, are close to those that have been reported previously for $Bi_2Te_3$. Specifically, the bismuth $4f_{7/2}$ peak is approximately 0.5 eV lower than literature precedents and the tellurium $3d_{5/2}$ peak is identical to literature precedents, within the resolution of these spectra, and we assign the peaks to $Bi_2Te_3$ in Figure 9. The two higher-binding-energy peaks at 158.2 and 575.6 eV are close to literature precedents for bismuth $4f_{7/2}$ and tellurium $3d_{5/2}$ of $Bi_2O_3$ and $TeO_2$, respectively, and we assign these peaks as oxide in Figure 9. On the basis of these assignments, our interpretation of the XPS spectra for freshly prepared $Bi_2Te_3$ nanowires is that these structures are quickly covered with a mixed bismuth and tellurium oxide layer resulting from the air oxidation at the surfaces of the $Bi_2Te_3$ nanowires. On the basis of the layered oxide structure model suggested by Bando et al.[53] and the inelastic mean free paths of the photoelectrons,[54] we estimate that within an hour of air exposure the oxide, on the freshly prepared nanowires, consists of layers of $Bi_2O_3$ and $TeO_2$ that are 2.2 and 1.1 nm thick, respectively.

**Table 1. Summary of XPS Analyses of $Bi_2Te_3$ Nanowires[a]**

| $Bi_2Te_3$ sample description | Bi $4f_{7/2}$ B.E. (eV) | | Te $3d_{5/2}$ B.E. (eV) | | Te/Bi ratio | Bi oxide ratio[f] |
|---|---|---|---|---|---|---|
| | $Bi_2Te_3$ | oxide | $Bi_2Te_3$ | oxide | | |
| fresh[b] | 156.7 | 158.2 | 572.4 | 575.6 | 5.1 | 1.9 |
| electrooxidized 400 s[c] | 156.7 | 158.2 | 572.4 | 575.7 | 4.6 | 1.2 |
| electrooxidized 800s | 156.8 | 158.3 | 572.6 | 575.8 | 15 | 1.0 |
| aged[d] | 156.5 | 158.1 | 572.4 | 575.6 | 3.6 | 0.3 |
| electrooxidized 400 s + aged[e] | 156.9 | 158.2 | 572.3 | 575.7 | 1.6 | 0.5 |
| electrooxidized 800 s + aged | n.a. | 158.2 | 572.9 | 575.8 | n.a. | 0.0 |

| sample | Bi $4f_{7/2}$ B.E. (eV) | Te $3d_{5/2}$ B. E. (eV) | Te/Bi ratio | Bi/O ratio |
|---|---|---|---|---|
| elemental Bi | 156.9[55]−157.1[56] | | | |
| elemental Te | | 572.7[57]−573.1[58] | | |
| $Bi_2Te_3$ | 157.1[59]−157.2[30,53,60] | 572.0[53],572.3[30] | 1.5 | |
| $Bi_2O_3$ | 158.5[60]−159.8[56] | | | 0.66 |
| $TeO_2$ | | 575.8[61]−576.5[62] | | |

[a] Reference data courtesy of the NIST Photoelectron Spectroscopy Database (http://srdata.nist.gov/xps/) and ref 49. [b] Fresh $Bi_2Te_3$ samples were analyzed by XPS within 1 to 2 h of synthesis. [c] $Bi_2Te_3$ nanowires were electrooxidized for 400 s immediately after synthesis and analyzed within 1 to 2 h. [d] Aged $Bi_2Te_3$ samples were analyzed after exposure to laboratory air for 1 week. [e] Electrooxidized 400 s + aged were electrooxidized for 400 s immediately after synthesis and analyzed by XPS after exposure to laboratory air for 1 week. [f] The Bi oxide ratio is the ratio of bismuth present as $Bi_2Te_3$ and bismuth present as oxide.

The atomic Te−Bi ratio is expected to be 1.5 for stoichiometric $Bi_2Te_3$, and XPS analysis yields a ratio of 5.1 for freshly synthesized nanowires that have not been electrooxidized. The high Te−Bi ratio suggests that much of the excess tellurium seen by EDX (see above) is concentrated at the surfaces of these nanowires, and this is consistent with the accumulation of tellurium at the surfaces of $Bi_2Te_3$ nanowires during the cyclic electrodeposition/stripping synthesis. The positive limit of 0.35 V is sufficient to remove excess bismuth from the nanowires by reaction 5 but not excess tellurium, which requires +0.55 V (Figure 2b). The source of this excess tellurium is most likely its incomplete reaction with $Bi^{3+}$ according to reaction 8.

Electrooxidation of the $Bi_2Te_3$ nanowires at +0.37 V for either 400 or 800 s did not alter the binding energies of either the Bi

(53) Bando, H.; Koizumi, K.; Oikawa, Y.; Daikohara, K.; Kulbachinskii, V. A.; Ozaki, H. *J. Phys.: Condens. Matter* **2000**, *12*, 5607.
(54) *NIST Electron Inelastic-Mean-Free-Path Database*, version 1.1; Powell, C. J., Jablonski, A., Eds.; National Institute of Standards and Technology: Gaithersburg, MD, 2001.
(55) Shalvoy, R. B.; Fisher, G. B.; Stiles, P. J. *Phys. Rev. B* **1977**, *15*, 2021.
(56) Dharmadhikari, V. S.; Sainkar, S. R.; Badrinarayan, S.; Goswami, A. *J. Electron. Spectrosc.* **1982**, *25*, 181.
(57) Mandale, a. B.; Badrinarayanan, S. *J. Electron. Spectrosc.* **1990**, *53*, 87.
(58) Bahl, M. K.; Watson, R. L.; Irgolic, K. J. *J. Chem. Phys.* **1977**, *66*, 5526.
(59) Ismail, F. M.; Hanafi, Z. M. *Z Phys. Chem. (Leipzig)* **1986**, *267*, 667.
(60) Debies, T. P.; Rabalais, J. W. *Chem. Phys.* **1977**, *20*, 277.
(61) SUN, T. S.; Buchner, S. P.; Byer, N. E. *J. Vac. Sci. Technol.* **1980**, *17*, 1067.
(62) Christie, A. B.; Lee, J.; Sutherland, I.; Walls, J. M. *Appl. Surf. Sci.* **1983**, *15*, 224.

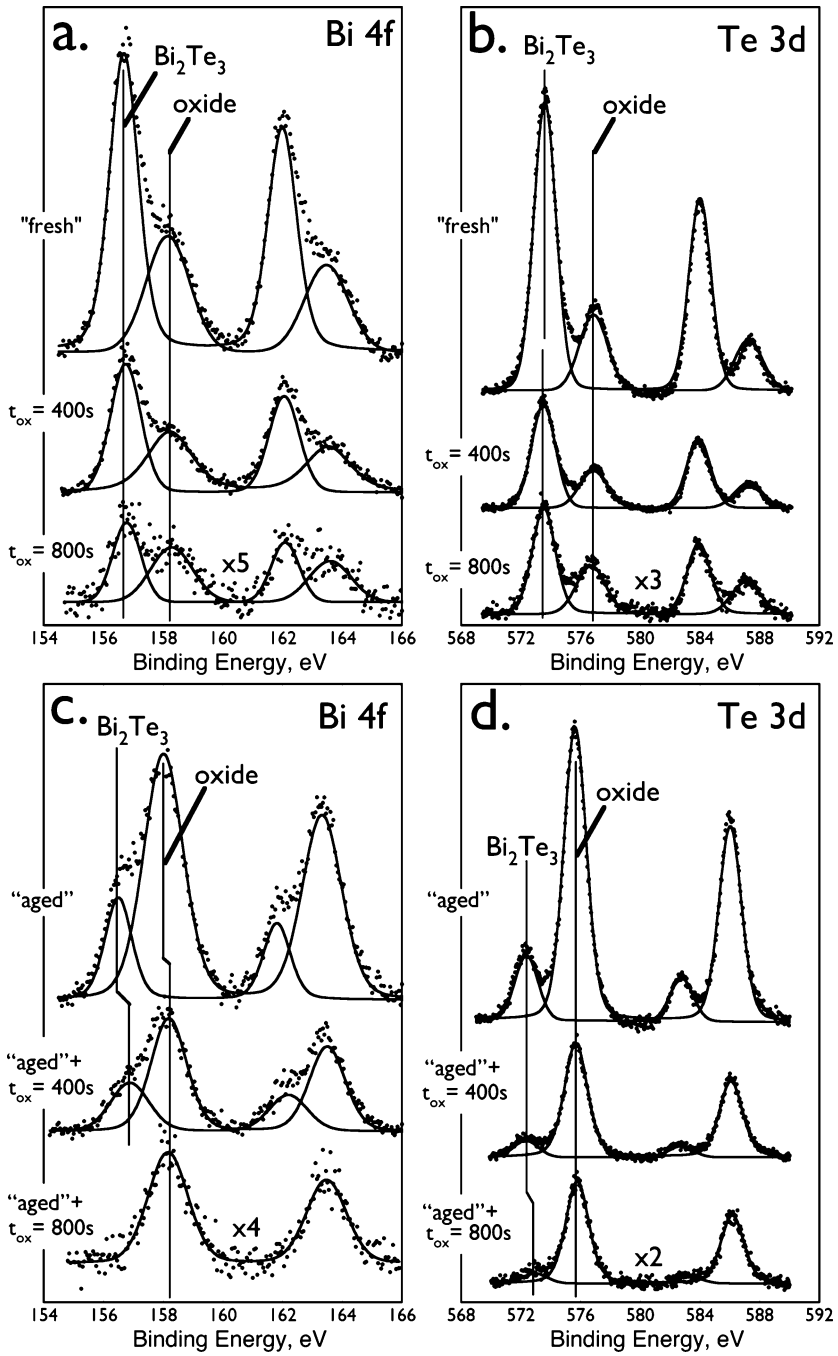


**Figure 9.** (a) XPS spectra of the bismuth 4f and tellurium 3d regions for $Bi_2Te_3$ samples prepared as follows: Three samples of 200-nm-diameter $Bi_2Te_3$ nanowires were prepared using 20 electrodeposition/stripping scans. One of these samples was electrooxidized at +0.37 V vs SCE for 400s, and one, for 800 s. The third sample was not electrooxidized. The spectra shown in a and b, labeled "fresh", were then acquired within 1 to 2 h. These same three samples were examined a second time by XPS after 1 week of exposure to laboratory air, resulting in the scans shown in c and d. The spectra for these samples are labeled "aged".

4f or Te 3d peak of the nanowires, indicating that a $Bi_2Te_3$ core remains after electrooxidation. There is, however, some evidence for the buildup of oxides on the surfaces of these nanowires during the etching process. First, a Te−Bi nanowire ratio of 15 was observed for the sample electrooxidized for 800 s. This suggests that under the kinetically controlled etching conditions the dissolution of excess elemental Te is slower than the dissolution of $Bi_2Te_3$ and that the oxidation of this Te may compete with the dissolution process. Second, the ratio between the Bi $4f_{7/2}$ peak area associated with the $Bi_2Te_3$ nanowires and that associated with the $Bi_2O_3$ decreases from 1.9 for the as-synthesized nanowires to 1.2 (electrooxidation for 400s) to 1.0 (800 s). The ratio of the tellurium $3d_{5/2}$ peak area of the $Bi_2Te_3$ nanowire to that of the $TeO_2$ follows a similar trend. The presence of these accumulated oxides will impede attempts to make high-quality electrical contacts to these nanowires.

We repeated the XPS analyses after the three samples probed in Figure 9a and b were aged in laboratory air for 1 week. These spectra are shown in Figure 9c and d. This aging process induced virtually no shifts in the binding energies of the Bi 4f and Te 3d peaks for either the nanowire or oxide chemical states (Table 1), but the abundance of the oxidized state was increased dramatically for all three samples. The $Bi_2Te_3$ nanowire−oxide ratio of the Bi 4f peak areas is decreased 6-fold for the fresh sample left to age 1 week and 2.5-fold for the sample that was electrooxidized for 400 s and left to oxidize for 1 week. The rate

of air oxidation seen here is significantly higher than that reported by Bando et al.,[53] who studied the rate of $Bi_2Te_3$ oxidation for the planar surfaces of single $Bi_2Te_3$ single crystals. The oxidation conditions employed in that study (30% relative humidity, 24 °C) were similar to the conditions prevailing in our laboratory during nanowire aging (~55% relative humidity, 20−23 °C). The total extent of oxidation, as evidenced by the oxide ratio measured either for Bi or Te, is also significantly higher here, and this translates into a thicker oxide layer. (The limiting oxide layer thickness seen by Bando was 1.2 nm for an oxidation time of 300 h.) It is likely that the relatively rapid oxidation that we observe for the nanowires in air is the result of the polycrystalline nature of the nanowires and the likelihood of high defect densities in the regions where the initial nanocrystals coalesce to form nanowires. The especially rapid surface oxidation of polycrystalline $Bi_2Te_3$ nanowires seen here provides an explanation for the irreproducibility and instability in the *ZT* values (e.g., Figure 8d) that we have measured for $Bi_2Te_3$ nanowire ensembles. It is clear, on the basis of this XPS analysis, that in order to establish high-quality electrical contacts to these nanowires it will be necessary to avoid the formation of this oxide.

## IV. Summary

Electrochemical step edge decoration has been used to electrodeposit polycrystalline $Bi_2Te_3$ nanowires with diameters in the range of 300 to 30 nm. In contrast to the template synthesis method, ESED produces nanowires that are much longer—more than 100 $\mu$m in length. On the basis of calculations that we have presented here, we believe that this attribute will be essential to the fabrication of high-performance TE devices based on nanowires. A second advantage is the horizontal orientation of these nanowires on the electrode surface and the ease with which they may be transferred to an electrically and thermally insulating surface. After transfer, metal contacts may be readily deposited onto ensembles of these nanowires, expediting the measurement of thermal properties. The analogous measurements for template-synthesized nanowires, oriented vertically on the electrode and encapsulated by the template, have proven to be much more difficult.

Other conclusions from this study are the following:

(1) A cyclic electrodeposition/stripping method is required in order to obtain near-stoichiometric $Bi_2Te_3$ nanowires by electrodeposition on graphite electrode surfaces. During electrodeposition by cyclic electrodeposition stripping, excess bismuth that is co-electrodeposited with $Bi_2Te_3$ is continually and selectively removed. However, smaller excesses of tellurium are not removed by this procedure.

(2) Kinetically controlled electrooxidation has been used to reduce the diameter of $Bi_2Te_3$ nanowires into the 30 nm range. The diameter distribution of $Bi_2Te_3$ nanowires unexpectedly becomes narrower during this process. In principle, this method can be used to reduce the diameter of $Bi_2Te_3$ nanowires prepared using any synthesis method.

(3) XRD, EDX, XPS, and electron diffraction analyses all support the conclusion that high-quality $Bi_2Te_3$ is produced by the technique described here. However, our XPS data clearly shows that exposure to laboratory air results in the formation of an oxide layer that is more than 1 nm in total thickness within a few hours. This oxide layer is rich in tellurium, suggesting that it is formed from the elemental tellurium that builds up during the electrodeposition/stripping synthesis process. The electrooxidation of $Bi_2Te_3$ nanowires accelerates the appearance of this surface oxide.

(4) Measurements of *ZT* on 40 transferred nanowire samples showed no detectable thermoelectric behavior for 37 of these samples and *ZT* values of 0.2, 0.72, and 0.82 for the remaining three samples. For one of these, the measured *ZT* was observed to decay rapidly from 0.82 to zero over a period of 2 days. In view of the good materials characterization metrics measured for these nanowires, we tentatively attribute the irreproducibility of the *ZT* measurement to the rapid formation in air of surface oxides that degrade the electrical contacts.

**Acknowledgment.** This work was funded by the National Science Foundation (grant DMR-0405477) and by the petroleum Research Fund administered by the American Chemical Society (grant 40714-AC5). J.C.H. acknowledges funding support from the Department of Energy (grant DE-FG03-96ER45576). Graphite for this work was supplied by a grant from the EU Commission FP6 NMP-3 project 505457-1 ULTRA-1D. We thank Professor Derek Dunn-Rankin of UCI Mechanical and Aerospace Engineering for helpful discussions.

LA061275G